PAPER • **OPEN ACCESS**

Rapid prototyping of a 3D well-shaped, porous, microelectrode array for extracellular recordings from cardiac cell layers and cortical organoids

To cite this article: Zeynep Izlen Erenoglu *et al* 2026 *Biofabrication* **18** 025005

Biofabrication

OPEN ACCESS

RECEIVED
30 October 2025

REVISED
11 January 2026

ACCEPTED FOR PUBLICATION
2 February 2026

PUBLISHED
3 March 2026

PAPER

Rapid prototyping of a 3D well-shaped, porous, microelectrode array for extracellular recordings from cardiac cell layers and cortical organoids

Zeynep Izlen Erenoglu[1,5], Lukas Hiendlmeier[1,2,5], Fulvia Del Duca[1,5], Inola Kopic[1], Sebastian Schmidt[3,4], Lennart J K Weiß[1], George Al Boustani[1,2], Tetsuhiko F Teshima[1,2], Gil Westmeyer[3,4] and Bernhard Wolfrum[1,2,*]

[1] Neuroelectronics, Munich Institute of Biomedical Engineering, Department of Electrical Engineering, School of Computation, Information, and Technology, Technical University of Munich, Hans-Piloty-Str. 1, 85748 Garching, Germany
[2] Medical & Health Informatics Laboratories, NTT Research Incorporated, Sunnyvale 94085, United States of America
[3] Neurobiological Engineering, Munich Institute of Biomedical Engineering, Department of Bioscience, TUM School of Natural Science & TUM School of Medicine, Boltzmannstraße 11, Garching, Germany
[4] Institute for Synthetic Biomedicine, Helmholtz Munich, Neuherberg, Germany
[5] These authors contributed equally.
[*] Author to whom any correspondence should be addressed.

E-mail: bernhard.wolfrum@tum.de

Keywords: microfabrication, neuroelectronics, microelectrode arrays, extracellular recording, electrogenic cells

Supplementary material for this article is available online

Abstract

Microelectrode arrays (MEAs) can be used to record extracellular field potentials of cells, enabling investigations on neural or cardiac cellular electrical activity. However, conventionally used 2D cell monolayers cannot recapitulate the 3D microenvironment of *in vivo* tissue. Therefore, cells are grown in 3D cultures that mimic the architectural and functional aspects of human organs. MEAs that support such 3D structures are of increasing importance, but their fabrication often relies on advanced cleanroom techniques. Here, we present a fast and straightforward prototyping technique for a thin-film, porous MEA fabricated using conformal coatings and laser ablation. The absence of photolithography processes allows the MEA to be directly fabricated as a 3D structure. This advantage was exploited by manufacturing 3D, well-shaped MEAs to host cortical organoids for extracellular signal recordings. The 3D-printing-based fabrication of the wells enables the tuning of the MEA shape according to the size of the organoid. The proposed well-shaped MEAs enable easy handling and secure organoid placement by physically retaining the organoid within the well, ensuring direct alignment with underlying electrodes, avoiding the detachment issues typically encountered on 2D MEA designs. We present extracellular field potential recordings from both cardiac cells and cortical organoids.

1. Introduction

Cardiac and neuronal cells utilize electrical signals as their primary means of interaction. The resulting extracellular field potentials and their interactions can be studied *in vitro* using microelectrode arrays (MEAs). MEAs enable non-invasive, simultaneous extracellular recording and stimulation with high spatial and temporal resolution, allowing for the study of network activity and connectivity. Some examples of studies using MEAs include investigations of field potential propagation in cardiac cells [1–6] and network dynamics in neural cells [7–11].

Conventionally, cells are grown on a flat surface where they adhere. However, 2D planar cell cultures on rigid surfaces do not accurately replicate the complex 3D environment of *in vivo* human tissue and do not provide ideal models for disease and drug research. Therefore, cell models have

been further developed into spheroids and organoids, which are three-dimensional, self-organized models with an architectural structure unique to the organ or tissue of interest. Specifically, when developed from induced pluripotent stem cells (iPSCs), they can differentiate into many different cell types, exhibiting tissue-like interactions between the cells [12–15]. Brain organoids can contribute to the understanding of neurodegenerative disorders such as Parkinson's and Alzheimer's disease, and partially reproduce the functional abnormalities these diseases cause [16–19]. However, commonly used flat MEAs pose challenges for recording electrophysiological data from the 3D organoids. When organoids are placed on planar electrode surfaces, they often drift or float away due to the lack of physical confinement, making secure positioning difficult. Moreover, signal acquisition is restricted to the bottom interface in contact with the electrodes, where nutrient diffusion is limited, and long-term viability can be compromised.

To measure electrical activity from such 3D cell models, the 2D MEAs must be modified. Ideally, the MEAs should be able to mechanically stabilize the organoid in place on top of the electrodes and ensure sufficient fluid and nutrient exchange at the electrode-organoid interface. As the conventionally used lithography-based fabrication of MEAs is limited to flat 2D structures, several advanced design strategies have been introduced to achieve a three-dimensional electrode-organoid interface. These include mesh-like electrodes around which the organoid can grow [20–22], structures that bulge upon organoid insertion [23], and foldable electrode systems that wrap around organoids and cell aggregates [24–28]. Although direct 3D patterning by photolithography is possible, it requires intricate design and fabrication strategies, limiting its broader adaptability [28, 29]. As an alternative, other 3D patterning techniques, such as inkjet printing, have been developed to interface with organoids, which involve the use of needle-like electrodes [30–34]. A simple alternative is the attachment of prefabricated polymeric well structures, such as PDMS well arrays, onto planar MEAs [35, 36]. While effective in preventing organoid displacement, the underlying MEA remains intrinsically two-dimensional, with confinement provided by an externally bonded structure. Consequently, this approach does not allow the fabrication of truly three-dimensional MEAs or the realization of alternative MEA geometries. Furthermore, ensuring nutrient exchange at the electrode-organoid interface is often limited and typically requires additional processing steps or the use of specific material combinations. Overall, these approaches typically rely on advanced and time-consuming fabrication workflows, are constrained to planar substrates, require cleanroom infrastructure, and involve the use of harsh chemicals.

The aim of this work was to develop a simple process that enables the direct fabrication of a three-dimensional, well-shaped MEA capable of mechanically stabilizing organoids at a porous recording site. The process should be readily adaptable to alternative MEA geometries, allowing for its use with various tissue configurations, such as organoid clusters.

Therefore, we report a novel fabrication strategy for 3D-shaped MEAs by combining 3D printing, parylene C deposition, and laser micro-machining (figure 1(a)). Using this approach, 3D-shaped MEAs can be fabricated in which the electrodes are distributed within a well-shaped structure designed for organoid placement. The presented 3D MEAs comprise a freestanding membrane with optional perforations that enable the diffusion of nutrients and oxygen, thereby maintaining the viability of the organoids (figure 1(b)). The fabrication process is simple and rapid, benefiting from the use of additive manufacturing and laser-based patterning, which allow straightforward design modifications and rapid prototyping. While the electrodes fabricated using this approach exhibit higher variability and reduced long-term stability compared to those produced by conventional lithography-based processes, the method enables the direct realization of three-dimensional well structures through a workflow with a reduced number of fabrication steps.

As a proof of concept, we fabricated a strainer-shaped MEA comprising 32 electrode sites each featuring perforations. Using this platform, we recorded electrophysiological signals from cortical organoids positioned within the 3D membrane wells, as well as from cardiomyocyte-like HL-1 cells.

2. Results

2.1. Fabrication

We fabricated the 3D well-shaped, membrane-like MEAs using the following fabrication strategy (figure 2(a)). First, a 3D-printed mold defines the 3D structure of the MEA, which is fabricated on the top surface of the mold. It is printed by Stereolithography (SLA), allowing a high-resolution mold structure (features >100 μm). To facilitate the release of the membrane from the mold, a water-soluble gelatin sacrificial layer is applied directly to the surface, allowing for the release of the layer afterward.

On top of the mold, the first parylene C layer is coated, acting as the substrate of the MEA (i). The overall fabrication relies on the ability to coat parylene C conformably on complex 3D designs, including those with undercuts. Parylene C is a polymer deposited by chemical vapor deposition (CVD) and is mechanically robust, biocompatible, and

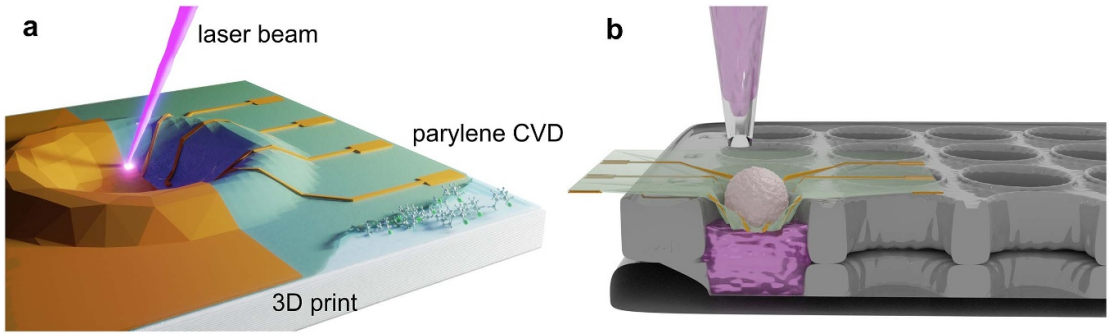

Figure 1. 3D well-shaped MEA. (a) Illustration of the main steps enabling the fabrication of custom-shaped 3D MEAs: a mold of the desired shape is 3D printed, a layer of parylene C is conformally deposited via CVD, and the conductive layer is sputtered and patterned by laser ablation. (b) Illustration of the proposed application of the 3D well-shaped MEA for electrophysiological recording from organoids.

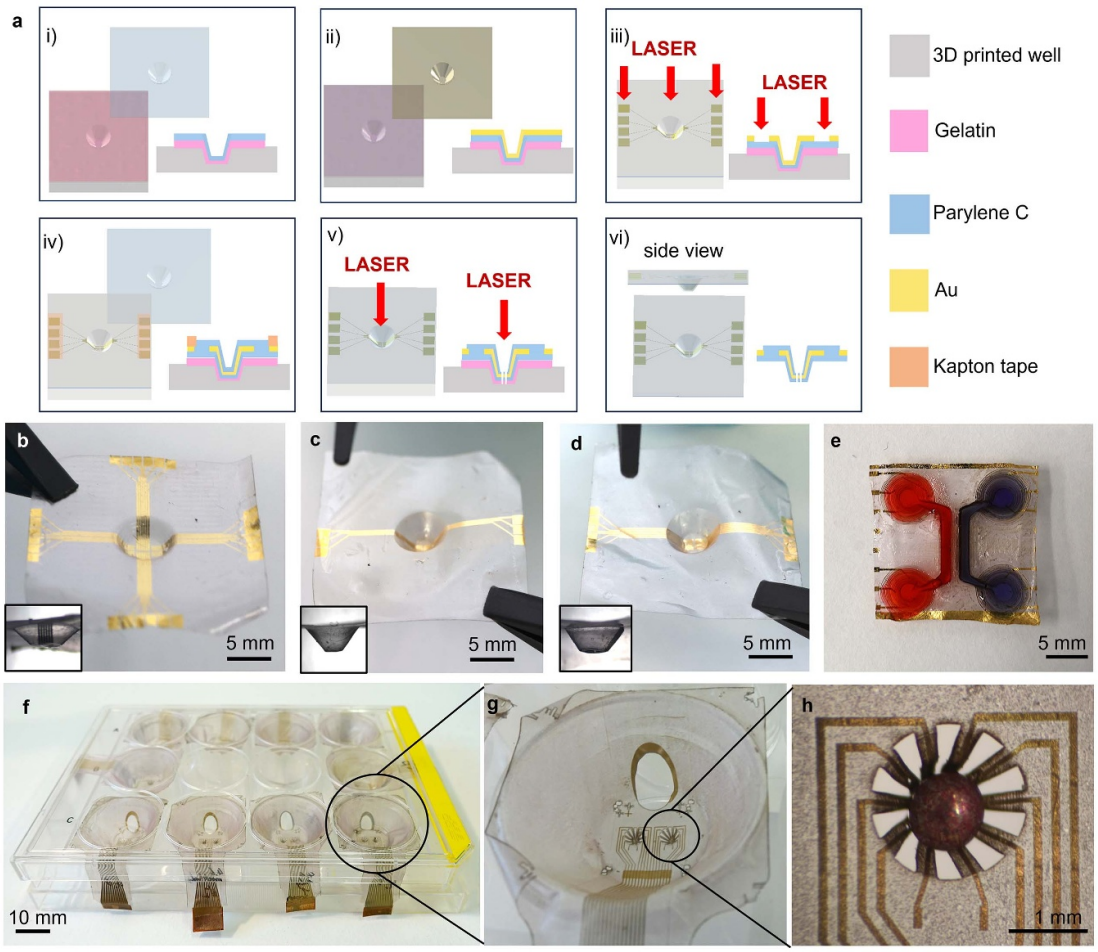

Figure 2. (a) Schematic illustration of the fabrication process to produce the 3D-shaped membrane MEAs: (i) deposition of the first parylene C layer onto the 3D-printed mold, separated by a sacrificial layer; (ii) sputtering of gold to form conductive traces; (iii) patterning of the gold layer by laser ablation; (iv) masking of the contact pads with Kapton tape followed by deposition of a top parylene C layer; (v) opening of the electrodes and pores by laser ablation; (vi) release of the freestanding membrane from the mold. (b) Fabricated MEA with 1 mm well depth and 3 mm bottom diameter, (c) 2 mm well depth and 2 mm bottom diameter, (d) 2 mm well depth and 3 mm bottom diameter. (e) Example of customizable well shapes and electrode distributions. Wells are partially filled with dyed liquid for illustration. (f)–(h) Strainer-shaped wells as inserts for standard multi-well plates, (h) featuring a glass bead to show the position of an organoid.

exhibits good dielectric properties [37]. Therefore, it is used to fabricate MEAs for biomedical applications [38]. In our 3D MEA, the layer of parylene C serves as the primary material for the freestanding membrane, acting both as the substrate and passivation material for the electrodes. While similar thin parylene devices

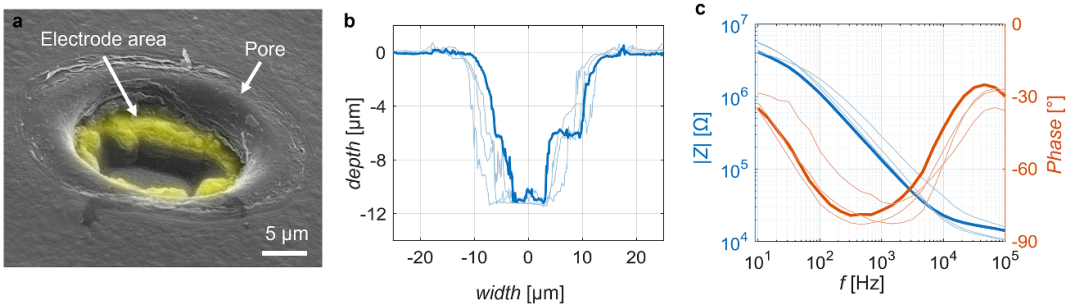

Figure 3. Characterization of the pore electrodes. (a) SEM image of an exemplary pore. (b) Exemplary depth profile of 4 representative (out of $n = 22$) pores (one example pore is highlighted). (c) Impedance spectroscopy data of 4 representative (out of $n = 18$ across 3 devices) pore electrodes (one example pore is highlighted).

are commonly used as flexible, conformal implants in planar configurations, parylene C exhibits a Young's modulus in the gigapascal range. Thus, when structured into a three-dimensional geometry, even a 10 μm thick layer provides sufficient mechanical stability to maintain the well shape during handling and cell culture [39].

Afterward, a conductive layer is deposited, in our case, by sputtering a layer of gold (Au) (ii). Rotating the device during the process ensured full coverage of the surface. Conventionally, the electrode layer of MEAs is patterned by photolithography. However, photolithography on 3D structured surfaces is challenging and not easily adaptable to changes in the 3D design. Therefore, we used a nanosecond pulsed UV laser scanner to pattern the metal layer on our MEAs (iii). This fabrication technique can be easily modified to accommodate different designs in a rapid prototyping mode. The pulse power and pulse frequency were chosen to selectively remove the higher absorbing metal without damaging the parylene C layer, which also slightly absorbs in the UV range [40]. The patterning fully removed the gold layer separating the traces, which was confirmed by measuring the direct current resistance between them. The ablation did not produce pinholes in the parylene C substrate layer, as verified by chronoamperometric measurements with a -2 V square waveform, confirming intact insulation of the electrodes. The laser features automatic focus adjustment over several centimeters, ensuring the laser spot remains well-defined on the 3D surface during patterning. However, full freedom of 3D patterning is still not possible with this technique. Patterning is limited to surfaces that are directly reachable by a straight laser beam; consequently, conductive areas in undercuts cannot be patterned. In the presented fabrication approach, the smallest achievable resolution, feedline width, and separation are constrained by the laser spot size ($\sim$24 μm in our system), whereas the total number of electrodes is determined by the available surface area and the chosen electrode layout. A single laser ablation line of 24 μm width was sufficient to provide reliable electrical isolation between adjacent traces, while feedlines remained reproducibly conductive down to widths of approximately two spot sizes. The MEAs used in the following experiments were designed with 200 μm wide feedlines and a 50 μm separation between them. After structuring the conductive layer, another parylene C layer was coated on top, acting as passivation, while masking the contact pads for connection with Kapton tape (iv). The electrode sites were opened by laser ablation as pores drilled through the material stack, thereby exposing a rim of gold that serves as the active electrode, as shown in figure 3(a). Direct removal of the low-absorbing parylene C passivation layer without ablating the underlying gold is not feasible, as this would require high-power lasers with short focal lengths that are incompatible with patterning on three-dimensional surfaces. For this purpose, increased laser power and repetition rate were used to ablate through the full stack of parylene C, Au, and parylene C. The laser parameters were optimized to ensure that the pores were opened throughout the entire thin film while minimizing damage to the surrounding areas. In the same processing step used to open the electrode sites, additional pores were ablated into the MEA membrane, and the outline of the 3D MEA was cut to release the structure from the mold (v).

In contrast to conventional lithographic processes, in which electrode sites are opened by selectively removing the passivation layer on top of the metal, exposing the conductive material through laser-cut pores offers several advantages. The process is fast (5 s for an array with 32 pores). Within the same step, additional pores can be laser-cut into the purely insulating parylene C layer to act as a sieve, facilitating nutrient exchange and allowing excess fluid to drain during organoid seeding. Moreover, this approach enables electrode openings on non-planar, three-dimensional geometries while relying on a single fabrication step. To release the parylene C stack from the mold and obtain the freestanding

3D membrane MEA, the structures are immersed in water at 50 °C for several hours (2–24 h), which dissolves the sacrificial layer (vi).

To demonstrate the flexibility of the fabrication towards different designs, we fabricated MEAs featuring wells with varying depths, diameters, and shapes (figures 2(b)–(d)) and other more complex example structures (figures 2(e)–(h)).

The released 3D membrane MEAs are fixed on a well for cell culture purposes, which serves as a fluid reservoir. When pipetting the organoids into the well, the membrane acts as a sieve to filter the organoid from the medium and keep it in place on top of the electrodes.

2.2. Characterization of the pore electrodes

We characterized the pore electrodes from laser drilling optically and electrochemically (figure 3). The exemplary depth profiles of a pore showed that the laser successfully ablated through the parylene C, Au, and parylene C stack (figure 3(b)).

The sizes of the pores were measured with a confocal laser profilometer, yielding a top diameter of 20 ± 2 μm and a bottom diameter of 10 ± 2 μm (mean and standard deviation $n = 24$) (figure 3(b)). Halfway through the layers, the pore diameter decreased and formed a rim, exposing the gold layer. This rim is the optically open electrode with an area of 240 ± 38 μm^2.

Electrical impedance spectroscopy (EIS) in PBS was performed to investigate the pores' electrochemical properties. For the analyzed electrodes, an average functional electrode yield of 73% ± 12% (mean ± SD; impedance at 1 kHz < 10 MΩ; $n = 117$ electrode sites across 4 devices) was achieved (figure S1). As seen in figure 3(c), the spectrum shows a capacitive influence in the region of 10^2–10^5 Hz, which we attribute to the double layer capacitance. The impedance at 1 kHz is 210 ± 120 kΩ ($n = 18$ working electrodes across 3 devices). Using an R(RC) simplified Randles circuit model, the capacitance of the electrode-electrolyte interface, 0.9 ± 0.5 nF, can be fitted to the EIS data. Assuming a capacity of ∼20–60 $\mu F\ cm^{-2}$ of a plain gold electrode, the electrochemically active electrode area is about 1000–4000 μm^2 [41]. The electrochemically determined electrode area is larger than the optically measured area, likely due to local lifting of the parylene C passivation around the pore during laser processing. This exposes additional gold surface within a region of approximately 40 μm in diameter, increasing the area in contact with the electrolyte. As expected for a rapid laser-based fabrication method, the measurements showed increased variability and batch-to-batch variation in the pore electrodes (figure S1) compared to cleanroom-fabricated electrodes, which can be attributed to the irregular and shape-variable nature of the laser-opened electrode sites. Nevertheless, the electrochemical characterization validated that the rim seen by the profilometry measurements reliably featured an open electrode, with impedances low enough for cell signal recording. To evaluate long-term electrode stability under cell culture conditions, impedance was measured at 1 kHz over four weeks at 37 °C in PBS, revealing a gradual decrease in the number of functional electrodes as well as average impedance, while the impedance values of the remaining functional electrodes stayed within the same order of magnitude (figure S2). Next, we evaluated the applicability of the electrodes for electrophysiological recordings *in vitro*.

2.3. Proof of concept in vitro

To assess the compatibility with cell culture and to characterize the performance of the created pore electrodes in an actual application, we first cultured a conventional planar cell layer of electroactive HL-1 cardiac cells for 3 d. To image the layer easily with the microscope, we produced a planar MEA using the same fabrication scheme on top of a flat mold, rather than a three-dimensional one.

Figure 4(a) shows the confluent layer of HL-1 cells on top of the MEA. The cells were stained with calcein acetoxymethyl (AM) to visualize viable cells. Comparable morphology and confluence were observed relative to control cultures, including in the vicinity of the pores. These results indicate that the laser-based fabrication process does not adversely affect cell adhesion or viability over the duration of culture and that cells can grow in close proximity to the pores, enabling effective electrical coupling. Next, we assessed the electrophysiological activity of the cells by imaging the Ca^{2+} signals after staining with the fluorescent calcium indicator Cal-520 AM ($n = 2$). The propagation map of a representative Ca^{2+} activity wave is shown in figure 4(b). The activity propagates from the top left to the bottom right of the snapshot area depicted by the heatmap. A mean propagation speed of 1.01 $\mu m\ ms^{-1}$ was calculated. Subsequently, the electrical signal recording capabilities were also assessed for confluent HL-1 cell layers on a 3D well-shaped MEA ($n = 5$). Therefore, we recorded extracellular signals amperometrically using a custom-built multi-channel transimpedance amplifier [42]. While the recordings presented here were performed amperometrically, the measured electrode impedances are also compatible with standard voltage recording approaches. Figure 4(c) shows the signal traces of the spontaneous periodic electrical activity of HL-1 cells, with a frequency of 0.84 Hz. After applying the denaturing agent sodium dodecyl sulfate (SDS), the beating signal could no longer be observed, verifying its cellular origin (figure 4(d)). These results are in line with those previously reported for HL-1 cell recordings [43]. The signal-to-noise level was approximately 27, with a noise level of 7.7 pA (root mean square). These values are comparable to those obtained with other non-cleanroom-fabricated MEAs [44].

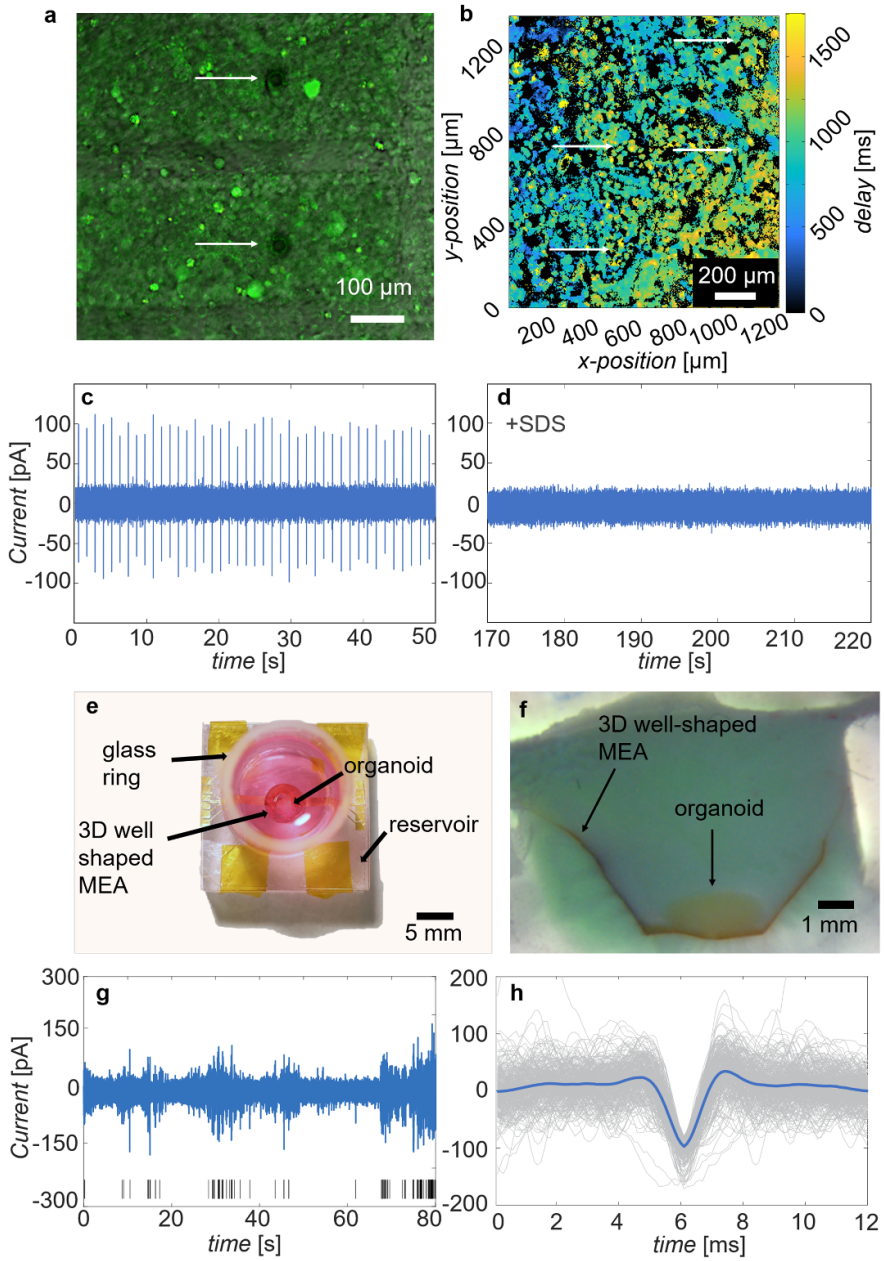

Figure 4. *In vitro* validation of 3D membrane MEAs. (a) Calcein dyed fluorescent images of a confluent HL-1 cell layer, showing good cell growth also over the pores. (b) Heatmap of Ca^{2+} signal propagation through the cell layer on a different sample. Arrows indicate the location of the pores. (c) Spontaneous electrical activity of the cardiac HL-1 cells measured by an active electrode representative of $n = 5$ biological replicates with 24 electrodes each. (d) Vanished signal after killing the cells with SDS. e) Cortical organoid positioned in the fabricated well MEA with 12 electrodes. (f) Corresponding cross-sectional view of the organoid after cryo-sectioning of the well MEA shown in e. The electrodes are not visible in the cross-sectional view. (g) Spontaneous signal bursts of the organoid and raster plot of the detected spikes, (h) traces of all detected spikes (gray, $n = 300$) and event-averaged waveform of all traces (blue).

In a separate experiment, to demonstrate that the device can resolve changes in cellular signaling relevant to pharmacological studies, 10 μl of 5 mM norepinephrine was added to the culture medium of the HL-1 cells. After recording a spontaneous beating frequency of 0.54 Hz, the addition of norepinephrine increased the beating frequency to 1.8 Hz, as shown in figure S3. The resulting signal-to-noise ratio was 21.3, while the noise level was 2.7 pA.

Finally, we also demonstrated the applicability of the MEAs to measure the activity of 3D cortical brain organoids. Therefore, organoids ($n = 4$ biological replicates) with a diameter of approximately 1–2 mm were selected from the culture and placed into a well MEA with the corresponding dimensions. The strainer-shaped membrane was fixed in a well that contains the culture medium and can be attached to the amplifier unit (figure 4(e)). The well shape holds the organoid in position, keeping it in close contact with the electrodes, as seen in the cross-section image in figure 4(f). The organoids were cultured in 3D-shaped well MEAs for 7 d *in vitro* (DIV),

and extracellular recordings were conducted using the amplifier system mentioned above. Spontaneous bursts of electrical activity were observed for two samples (figures 4(g) and (h)). The extracellular readout signals were high-pass filtered (100 Hz) for better distinction of the spontaneous bursts of electrical activity [45]. In contrast to HL-1 cells, the raw field potential signals from brain organoids are in the form of bursts of electrical activity, as we record compound activity from a cell network rather than regular peaks of action potentials, as observed with 2D cardiac cell monolayers. [32, 46–48].

Organoids with diameters of 1 mm or larger are known to frequently develop hypoxic and, in some cases, necrotic cores due to diffusion limitations. Accordingly, the organoids investigated here may also exhibit hypoxic core regions. Although histological stainings did not reveal pronounced alterations in cell-type composition in the organoid centers (figure S4), this does not exclude the presence of hypoxia. Notably, spontaneous electrophysiological activity was observed only in mature organoids with diameters exceeding 1 mm. On non-porous planar MEAs, limited nutrient and oxygen supply at the electrode-tissue interface on the bottom side of such organoids may compromise the viability and activity of cells in contact with the electrodes. In contrast, the porous MEA design used here enables medium access at the electrode-organoid interface, supporting the viability and activity of the outer shell of the organoid interfacing with the electrodes, even in the presence of a potentially hypoxic core.

3. Conclusion

We have reported a novel fabrication technique to create 3D well-shaped MEAs for 3D cell culture interfacing applications.

The proposed fabrication method is fast and relies solely on well-established biocompatible materials, including noble metals and parylene C. Thanks to the process being based on 3D-printed molds, the final electrodes can be fabricated in virtually any 3D shape that does not feature patterned undercuts.

Specifically, we have shown 3D MEAs fabricated in a tunable well shape to trap 3D cell cultures, such as cortical organoids, and record from them. The recording sites are pore electrodes that have been fabricated by laser ablation. The pores at the electrode sites are completely open through the parylene C membrane, acting as sieves to facilitate the exchange of nutrients between the cells and the medium, and promote an intimate connection between the cells and the electrode sites. We first verified the functionality of those active electrode sites by recording electrical signals from a layer of cardiomyocyte-like cells. Subsequently, we utilized a three-dimensional, well-shaped MEA to acquire recordings from cortical organoids.

When compared with lithographically fabricated arrays, the laser-based fabrication process presented here exhibits a clear trade-off. Lithography enables substantially higher resolution, allowing reduced feedline widths, higher electrode densities, and more precisely defined electrode openings. In contrast, the laser-based process enables the direct fabrication of three-dimensional MEA geometries, combining patterning and electrode opening into a single, straightforward processing step. With more advanced laser systems featuring smaller spot sizes, it is likely that reduced feature sizes and increased electrode densities, comparable to those of optical lithography, could be realized [49].

While this work primarily focuses on fabrication and the biological experiments serve as a proof of concept, we believe that this technology provides a customizable and scalable platform for systematic electrophysiological studies of organoids. Such a platform may ultimately enable improved disease models, including those based on patient-derived cells, particularly for investigating disorders in which electrical signaling pathways are affected [50–52].

4. Experimental section/methods

Materials: Claycomb medium, L-Glutamine solution, penicillin/streptomycin, norepinephrine bitartrate, fibronectin, gelatine from bovine skin, trypsin ethylenediaminetetraacetic acid (EDTA), Dulbeccos's phosphate saline (PBS 1×), SDS powder, H_2SO_4 (95%–98%), HL-1 cells and cAMP were acquired from Sigma-Aldrich (USA). Fetal bovine serum, Calcein AM, Geltrex Matrix, collagenase IV, and low attachment 6-well plates were bought from ThermoFisher Scientific (USA). Cal-520 AM dye was acquired from Biomol (Germany). Polydimethylsiloxane (PDMS Sylgard 184 (10:1 w/s base/curing agent)) and Matrigel Matrix were purchased from Dow Corning (USA). 2-Propanol (99.5%), ethanol (99.5%), and L-ascorbic acid were purchased from Carl Roth (Germany). Medicalprint Clear resin (385 nm) was obtained from Detax GmbH Co. KG (Germany), whereas the water-soluble PVA filament was acquired from Filamentworld (Germany). The silane A174 adhesion promoter was purchased from Plasma Parylene Systems GmbH (Germany). Deionized water was taken from Ultra Clear purification system/Berry Tec (Germany). StemMACS™ iPS-Brew XF (human), dorsomorphin, SHH, SB 431 542, BDNF, and GDNF were purchased from Milteyni Biotec (Germany). 20% Knockout serum replacement, GlutaMAX, NEAA, 2-Mercaptoethanol, DMEM/F12 (11330-032), N2 supplement, B27, and Neurobasal medium were bought from Life

Technologies (USA). A-83 and CHIR 99 021 were acquired from Tocris Bioscience (United Kingdom).

3D printing: the SLA-printed molds were manufactured with a MiiCraft 50X 3D printer (MiiCraft, Taiwan) from CAD files designed in Inventor (2022, Autodesk, USA). The samples were printed with a layer height of 10 μm and an exposure time of 1.4 s per layer in medical print clear. After printing, the molds were cleaned in 2-propanol in an ultrasonic bath for 5 min and were blow-dried. Finally, the molds were post-cured in an Otoflash G171 UV-curing chamber (NK-Optic, Germany) with 2000 flashes under nitrogen flux.

Sacrificial layer coating: a sacrificial layer was coated on top of the SLA printed molds. Therefore, we first diluted 2.5 g of gelatin in 47.6 ml of deionized water in a glass bottle and left it to dissolve on a hotplate at 50 °C for 4 h while stirring. The preparation was transferred in 2 ml Eppendorf tubes, spun for 90 s at 1200 rpm (miniSpin plus, Eppendorf, Germany), filtered with a 0.2 μm syringe filter (Whatman GD/X 13, Sigma Aldrich, USA) and transferred in a large petri dish. The surface of the mold was activated in oxygen plasma (Diener Femto Asher, Diener Electronic, Germany) at 0.6 mbar and 80% power for 20 min. Each mold was fully immersed in the solution for 1 min at 50 °C and was consecutively dried in vacuum overnight.

Electrode fabrication: a 5 μm-thick parylene C layer was deposited via CVD (Plasma Parylene Systems, Germany) from 16.7 g of dimer precursor (Daisan Kasei, Japan), with 3 Pa as deposition chamber pressure and 175 °C as the final temperature of dimer evaporation. Then, 100 nm of Au were sputtered (30 mA, 3 $\times$ 10^{-2} mbar, Bal-tec MED 020, Lichtenstein) and patterned by a nanosecond pulsed laser scanner (MD-U1000, Keyence, Japan, 5% power, 1000 mm s^{-1} speed, 60 kHz frequency and 5 repetitions). To coat the top passivation layer of the parylene C stack, the patterned layer was first treated by oxygen plasma and 200 μl of the adhesion promoter Silane A-174 in the deposition chamber and subsequently coated with 5 μm parylene C. The contact pads were masked with Kapton tape (Sigma Aldrich, USA) prior to deposition of the parylene C passivation. After the deposition of the insulation layer, the porous electrodes were opened with the MD-U1000C marking laser using 100% power, 1000 mm s^{-1} speed, 300 kHz frequency and 400 repetitions. The outline of the MEA was cut with the laser using 15% power, 500 mm s^{-1} speed, 40 kHz frequency, and 40 repetitions. The thin-film MEAs were released by immersion in deionized water at 50 °C for at least 2 h or until the sacrificial layer was completely dissolved.

Imaging: a 3D laser scanning confocal microscope (VK-X250, Keyence, Japan) with a 150$\times$ objective was used to image the electrodes. The images were analyzed using MultiFile Analyzer (Keyence, Japan). For the SEM images, the samples were first sputtered with 8 nm of gold (30 mA, 5 $\times$ 10^{-2} mbar). The samples were fixed on holders with a conductive double-sided carbon pad and copper tape and afterward imaged with the scanning electron microscope (JSM-6060LV, JEOL, Japan). The obtained images were processed in ImageJ. [53]

Electrochemical characterization: before characterization, glass rings with a diameter of 14.5 mm were attached to the top of the MEAs to serve as an electrolyte reservoir. Therefore, the rings were dipped into PDMS and placed on top of the chips, which were then cured in the oven for 1 h at 80 °C. Cyclic voltammetry, impedance spectroscopy, and chronoamperometry were performed on the chips using a potentiostat (VSP-300, BioLogic Science Instruments, France) in a three-electrode setup with an Ag/AgCl (3 M NaCl) reference electrode (BASI, United Kingdom) and a platinum coil wire as the counter electrode. The sample surfaces were cleaned and activated in 0.2 M H_2SO_4 by conducting CV sweeps across -0.4 V to 1.4 V with a scan rate of 500 mV s^{-1} and 100–300 cycles, depending on when a stabilized current response was reached. Impedance spectroscopy recordings were conducted by applying a sinusoidal signal with an amplitude of 10 mV at 0 V versus the open-circuit potential, and frequencies ranging from 1 Hz to 1 MHz.

HL-1 cell culture: HL-1 cells were cultured with Claycomb medium supplemented with 10% fetal bovine serum, penicillin/streptomycin (100 μg ml^{-1}), 0.1 mm of norepinephrine dissolved in fresh ascorbic acid solution, and 2 mm L-Glutamine and stored in a humidified incubator (37 °C, 5% CO_2; CB210 CO_2, Binder, Germany). After the seeded cells reached confluency and displayed mechanical beating patterns in T75 flasks, they were detached from the surface by adding 0.05% Trypsin/EDTA solution and resuspended in Claycomb medium. Subsequently, the cells were counted using a Neubauer chamber. Before seeding HL-1 cells on the chips, the chips were sterilized by dipping them into 2-propanol and air-drying. Afterward, they were treated with O_2 plasma (0.8 mbar, 80% power, 5 min, Diener Femto Asher, Diener Electronic, Germany) to hydrophilize their surface. The chips were then incubated in a solution containing fibronectin (5 μg ml^{-1}) and gelatin (0.2 mg ml^{-1}) for approximately 1 h in the incubator. The remaining coating solution was then removed and replaced with 80 000 HL-1 cells per cm^2 suspended in 500 μl of Claycomb medium. The

HL-1 cells were grown on the porous MEA chips for 3 d *in vitro* until a confluent layer was reached. An inverted microscope (Axiovert 40 CFL, Carl Zeiss, Germany) was used for the optical evaluation of cell growth and mechanical beating.

Cortical organoids: cortical organoids were differentiated according to a protocol published by Qian *et al* [54]. In brief, human hiPSCs from the line ISFi001-A (RRID:CVCL_YT30) were maintained on Geltrex coating and in human iPS-Brew XF at 37 °C, 7% CO_2, and 21% O_2. If not indicated otherwise, the medium was changed daily. Upon reaching a colony size of around 1.5 mm, colonies were detached using a 2 mg ml^{-1} collagenase IV solution for 45–60 min and incubated in iPS-Brew XF medium for 24 h in low-attachment 6-well plates on a 3D-Rocker/shaker at 37 °C, 5% CO_2, and 21% O_2. The next day, the medium was replaced by the first forebrain-specific medium [20% Knockout serum replacement, 1× GlutaMAX, 1× NEAA, 0.02% 2-mercaptoethanol, 1× penicillin-streptomycin, 2 μm dorsomorphin, 2 μm A-83, 100 ng ml^{-1} SHH in DMEM/F12]. At day 5, medium was replaced by the second forebrain-specific medium [1× N2 supplement, 1× GlutaMAX, 1× NEAA, 1× penicillin-streptomycin, 1 μm CHIR, 1 μm SB 431 542 in DMEM/F12]. At day 7, the formed embryoid bodies (EBs) were embedded in Matrigel and spread as a 1 mm thin sheet, forming a 'cookie' with the EBs distributed evenly inside. They are cultivated in the Matrigel 'cookie' for 5 d in the second forebrain-specific medium at 37 °C, 5% CO2, and 21% O_2, but not on the 3D-Rocker/shaker. On day 14, organoids were released from the cookie using a 5 ml pipette tip. The medium was replaced by the third forebrain-specific medium [1× N2 supplement, 1×B27, 1× GlutaMAX, 1× NEAA, 1× penicillin-streptomycin in DMEM/F12]. Organoids were transferred into a low-attachment 6-well plate and incubated on a 3D-Rocker/shaker at 37 °C, 5% CO_2, and 21% O_2 with medium changes every third day. On day 35, Matrigel (1:100) was added to the third forebrain-specific medium. At day 70, the medium was changed to the fourth forebrain-specific medium [1× B27 supplement, 1× GlutaMAX, 1× NEAA, 1× penicillin-streptomycin, 200 μm L-ascorbic acid, 500 μm cAMP, 20 ng ml^{-1} BDNF, 20 ng ml^{-1} GDNF in Neurobasal medium] with medium changes every fourth day.

After 70 and 100 d of organoid maturation, the organoids were gently placed in the wells of the thin-film, porous 3D-printed well MEAs using a pipette tip. The preparation of the 3D-printed well MEAs prior to organoid seeding followed a similar procedure to the experiments with HL-1 cells, which included drying in 2-propanol, O_2 plasma treatment, and overnight incubation in a Geltrex (120–180 μg ml^{-1} in DMEM/F12) coating solution. Prior to the Geltrex coating, the pipettes were cooled to prevent any gelation. The organoids were cultured on the MEAs for 7 DIV and the fourth forebrain-specific medium was changed every second day. At 7 DIV, extracellular recording experiments were conducted. For the cross-sectional images, the organoids within the thin-film porous 3D-printed well MEAs were fixed and cryosectioned for visualization following standard procedures [55, 56].

Fluorescent labeling: 4 mm Calcein-AM stock solution was diluted to a final concentration of 4 μm with either Claycomb medium or PBS. The old medium on the MEAs was aspirated and replaced with the staining solution. The devices were incubated for 15 min. Afterward, the staining solution was aspirated, washed with PBS, and replaced with fresh medium. The devices were then incubated for an additional 10 min. For imaging, the Leica DM2700M (Leica Microsystems, Germany) upright fluorescence microscope, equipped with a CoolLED p-E4000 light source (CoolLED, United Kingdom), was used with an immersion objective. First, a bright-field DIC image of the cells was taken with an inserted polarizer/analyzer and DIC prism. Next, the polarizer/analyzer and the prism were removed to take fluorescent images in the same position. For the fluorescent images, the cells were illuminated at around 490 nm. The images were processed in the LAS X software (Leica Microsystems GmbH, Germany) and overlaid in MATLAB (MathWorks, USA). For imaging calcium signals, the cell culture medium was changed 1 h prior to the experiment. 10 μm Cal-520 AM staining solution was added. The chips were first kept for 1 h in the humidified incubator and then for 30 min at room temperature. The staining medium was aspirated, and chips were washed with PBS and filled with fresh medium before being transferred to the imaging setup. For the imaging procedure, a Leica DFC9000GT sCMOS camera (Leica Microsystems, Germany) and the MicroManager software were used [57]. The propagation image stacks were captured with 3 × 3 binning, a 10 ms exposure time, a 70 ms interval, and consisted of 400 frames. The obtained images were viewed in ImageJ [53] and the data analysis was performed in MATLAB (MathWorks, USA).

Extracellular recordings: after 3 DIV, extracellular signals were recorded amperometrically using an in-house-built 64-channel amplifier shielded in a Faraday cage. An adapter was designed in Inventor (Autodesk, Inc., San Rafael, USA) to interface with the 3D well electrodes with the recording setup. The socket adapter was printed with the 3D-printer Ultimaker S3 using PLA Plus filament (Filamentworld, Germany). The amplifier features a 10 kHz sampling rate and a 1 GΩ feedback resistor. Before the experiment, 1% SDS solution was prepared in DI water. The medium was exchanged 1 h prior to the experiments with Claycomb medium

without norepinephrine. The recordings were conducted using an Ag/AgCl reference electrode. First, the spontaneous activity of the HL-1 cells and cortical organoids was recorded. Then, 150 μl (1% w/v) SDS solution was added to the medium to denature the cell membrane and stop any electrical activity from the cells. The measurement lasted approximately 1–5 min. The data analysis was conducted in MATLAB (MathWorks, USA).

Data availability statement

All data that support the findings of this study are included within the article (and any supplementary files), raw data sets are available under DOI: http://doi.org/10.5281/zenodo.18184436.

Rapid Prototyping 3D Well MEA available at http://doi.org/10.1088/1758-5090/ae40a0/data1.

Acknowledgments

The authors acknowledge funding by the Federal Ministry of Research, Technology and Space (BMFTR) and the Free State of Bavaria under the Excellence Strategy of the Federal Government and the Länder through the TUM Innovation Network: NEUROTECH and the ONE MUNICH Project Munich Multiscale Biofabrication. The authors also acknowledge funding from BMFTR through the PRISTINE project.

ORCID iDs

Zeynep Izlen Erenoglu 0009-0005-1129-4221
Lukas Hiendlmeier 0000-0003-0219-6871
Fulvia Del Duca 0000-0002-6684-173X
Inola Kopic 0000-0002-4147-462X
Sebastian Schmidt 0000-0003-4408-6697
Lennart J K Weiß 0000-0002-6943-737X
George Al Boustani 0000-0003-2723-8011
Tetsuhiko F Teshima 0000-0002-9462-7167
Gil Westmeyer 0000-0001-7224-8919
Bernhard Wolfrum 0000-0003-4438-3755

References

[1] Connolly P, Clark P, Curtis A, Dow J and Wilkinson C 1990 An extracellular microelectrode array for monitoring electrogenic cells in culture *Biosens. Bioelectron.* **5** 223–34
[2] Czeschik A, Rinklin P, Derra U, Ullmann S, Holik P, Steltenkamp S, Offenhäusser A and Wolfrum B 2015 Nanostructured cavity devices for extracellular stimulation of HL-1 cells *Nanoscale* **7** 9275–81
[3] Bachmann B, Adly N Y, Schnitker J, Yakushenko A, Rinklin P, Offenhäusser A and Wolfrum B 2017 All-inkjet-printed gold microelectrode arrays for extracellular recording of action potentials *Flex. Print. Electron.* **2** 035003
[4] Lee S *et al* 2019 Ultrasoft electronics to monitor dynamically pulsing cardiomyocytes *Nat. Nanotechnol.* **14** 156–60
[5] Ahadian S, Ramón-Azcón J, Ostrovidov S, Camci-Unal G, Hosseini V, Kaji H, Ino K, Shiku H, Khademhosseini A and Matsue T 2012 Interdigitated array of Pt electrodes for electrical stimulation and engineering of aligned muscle tissue *Lab Chip* **12** 3491–503
[6] Lin Z *et al* 2023 Tissue-embedded stretchable nanoelectronics reveal endothelial cell–mediated electrical maturation of human 3D cardiac microtissues *Sci. Adv.* **9** eade8513
[7] Borkholder D, Bao J, Maluf N, Perl E and Kovacs G 1997 Microelectrode arrays for stimulation of neural slice preparations *J. Neurosci. Methods* **77** 61–66
[8] Gross G W, Williams A N and Lucas J H 1982 Recording of spontaneous activity with photoetched microelectrode surfaces from mouse spinal neurons in culture *J. Neurosci. Methods* **5** 13–22
[9] Regehr W G, Pine J, Cohan C S, Mischke M D and Tank D W 1989 Sealing cultured invertebrate neurons to embedded dish electrodes facilitates long-term stimulation and recording *J. Neurosci. Methods* **30** 91–106
[10] Shein-Idelson M, Pammer L, Hemberger M and Laurent G 2017 Large-scale mapping of cortical synaptic projections with extracellular electrode arrays *Nat. Methods* **14** 882–90
[11] Zhao S, Tang X, Tian W, Partarrieu S, Liu R, Shen H, Lee J, Guo S, Lin Z and Liu J 2023 Tracking neural activity from the same cells during the entire adult life of mice *Nat. Neurosci.* **26** 696–710
[12] Ebert A D, Liang P and Wu J C 2012 Induced pluripotent stem cells as a disease modeling and drug screening platform *J. Cardiovasc. Pharmacol.* **60** 408–16
[13] Avior Y, Sagi I and Benvenisty N 2016 Pluripotent stem cells in disease modelling and drug discovery *Nat. Rev. Mol. Cell Biol.* **17** 170–82
[14] Liu C, Oikonomopoulos A, Sayed N and Wu J C 2018 Modeling human diseases with induced pluripotent stem cells: from 2D to 3D and beyond *Development* **145** dev156166
[15] Pastrana E 2013 The developing human brain—modeled in a dish *Nat. Methods* **10** 929
[16] Monzel A S *et al* 2017 Derivation of human midbrain-specific organoids from neuroepithelial stem cells *Stem Cell Rep.* **8** 1144–54
[17] Xiang Y *et al* 2017 Fusion of regionally specified hPSC-derived organoids models human brain development and interneuron migration *Cell Stem Cell* **21** 383–98.e7
[18] Adams J W, Cugola F R and Muotri A R 2019 Brain organoids as tools for modeling human neurodevelopmental disorders *Physiology* **34** 365–75
[19] Jo J *et al* 2016 Midbrain-like organoids from human pluripotent stem cells contain functional dopaminergic and neuromelanin-producing neurons *Cell Stem Cell* **19** 248–57
[20] Le Floch P, Li Q, Lin Z, Zhao S, Liu R, Tasnim K, Jiang H and Liu J 2022 Stretchable mesh nanoelectronics for 3D single-cell chronic electrophysiology from developing brain organoids *Adv. Mater.* **34** 2106829
[21] Li Q, Nan K, Le Floch P, Lin Z, Sheng H, Blum T S and Liu J 2019 Cyborg organoids: implantation of nanoelectronics via organogenesis for tissue-wide electrophysiology *Nano Lett.* **19** 5781–9
[22] Kim E *et al* 2025 Magnetically reshapable 3D multi-electrode arrays of liquid metals for electrophysiological analysis of brain organoids *Nat. Commun.* **16** 2011
[23] Li T L, Liu Y, Forro C, Yang X, Beker L, Bao Z, Cui B and Paşca S P 2022 Stretchable mesh microelectronics for the biointegration and stimulation of human neural organoids *Biomaterials* **290** 121825
[24] Cools J, Jin Q, Yoon E, Alba Burbano D, Luo Z, Cuypers D, Callewaert G, Braeken D and Gracias D H 2018 A micropatterned multielectrode shell for 3D spatiotemporal recording from live cells *Adv. Sci.* **5** 1700731
[25] Kalmykov A *et al* 2019 Organ-on-e-chip: three-dimensional self-rolled biosensor array for electrical interrogations of human electrogenic spheroids *Sci. Adv.* **5** eaax0729
[26] Park Y *et al* 2021 Three-dimensional, multifunctional neural interfaces for cortical spheroids and engineered assembloids *Sci. Adv.* **7** eabf9153

[27] Rich S I, Jiang Z, Fukuda K and Someya T 2021 Well-rounded devices: the fabrication of electronics on curved surfaces–a review *Mater. Horiz.* **8** 1926–58
[28] Yang X *et al* 2024 Kirigami electronics for long-term electrophysiological recording of human neural organoids and assembloids *Nat. Biotechnol.* **42** 1836–43
[29] Huang Q *et al* 2022 Shell microelectrode arrays (MEAs) for brain organoids *Sci. Adv.* **8** eabq5031
[30] Kim M *et al* 2022 Multimodal characterization of cardiac organoids using integrations of pressure-sensitive transistor arrays with three-dimensional liquid metal electrodes *Nano Lett.* **22** 7892–901
[31] Soscia D A, Lam D, Tooker A C, Enright H A, Triplett M, Karande P, Peters S K G, Sales A P, Wheeler E K and Fischer N O 2020 A flexible 3-dimensional microelectrode array for *in vitro* brain models *Lab Chip* **20** 901–11
[32] Sharf T *et al* 2022 Functional neuronal circuitry and oscillatory dynamics in human brain organoids *Nat. Commun.* **13** 4403
[33] Kopic I, Peng H, Schmidt S, Berezin O, Wang S, Westmeyer G G and Wolfrum B 2025 Inkjet-printed 3D sensor arrays with FIB-induced electrode refinement for low-noise amperometric recordings in hiPSC-derived brain organoids *ACS Sens.* **10** 6426–35
[34] Zips S *et al* 2023 Aerosol jet-printed high-aspect ratio micro-needle electrode arrays applied for human cerebral organoids and 3D neurospheroid networks *ACS Appl. Mater. Interfaces* **15** 35950–61
[35] Osaki T, Duenki T, Chow S Y A, Ikegami Y, Beaubois R, Levi T, Nakagawa-Tamagawa N, Hirano Y and Ikeuchi Y 2024 Complex activity and short-term plasticity of human cerebral organoids reciprocally connected with axons *Nat. Commun.* **15** 2945
[36] Sifringer L *et al* 2025 An implantable biohybrid neural interface toward synaptic deep brain stimulation *Adv. Funct. Mater.* **35** 2416557
[37] Kim B J and Meng E 2016 Micromachining of Parylene C for bioMEMS *Polym. Adv. Technol.* **27** 564–76
[38] Hassler C, von Metzen R P, Ruther P and Stieglitz T 2010 Characterization of parylene C as an encapsulation material for implanted neural prostheses *J. Biomed. Mater. Res. B* **93B** 266–74
[39] Sim W, Kim B, Choi B and Park J-O 2005 Theoretical and experimental studies on the parylene diaphragms for microdevices *Microsyst. Technol.* **11** 11–15
[40] Bera M, Rivaton A, Gandon C and Gardette J 2000 Comparison of the photodegradation of parylene C and parylene N *Eur. Polym. J.* **36** 1765–77
[41] Pajkossy T, Wandlowski T and Kolb D M 1996 Impedance aspects of anion adsorption on gold single crystal electrodes *J. Electroanal. Chem.* **414** 209–20
[42] Yakushenko A, Kätelhön E and Wolfrum B 2013 Parallel on-chip analysis of single vesicle neurotransmitter release *Anal. Chem.* **85** 5483–90
[43] Wells S P, Waddell H M, Sim C B, Lim S Y, Bernasochi G B, Pavlovic D, Kirchhof P, Porrello E R, Delbridge L M D and Bell J R 2019 Making cell culture more physiological: cardiomyocyte functional screening: interrogating comparative electrophysiology of high-throughput model cell systems *Am. J. Physiol. Cell Physiol.* **317** C1256–67
[44] Zips S, Grob L, Rinklin P, Terkan K, Adly N Y, Weiß L J K, Mayer D and Wolfrum B 2019 Fully printed μ-needle electrode array from conductive polymer ink for bioelectronic applications *ACS Appl. Mater. Interfaces* **11** 32778–86
[45] Passaro A P and Stice S L 2021 Electrophysiological analysis of brain organoids: current approaches and advancements *Front. Neurosci.* **14** 622137
[46] Tasnim K and Liu J 2022 Emerging bioelectronics for brain organoid electrophysiology *J. Mol. Biol.* **434** 167165
[47] Trujillo C A *et al* 2019 Complex oscillatory waves emerging from cortical organoids model early human brain network development *Cell Stem Cell* **25** 558–69.e7
[48] Kepecs A and Wang X-J 2000 Analysis of complex bursting in cortical pyramidal neuron models *Neurocomputing* **32** 181–7
[49] Troughton J and Proctor C 2025 Laser micromachining for bioelectronics: past, present, and future *Small Methods* **10** e01560
[50] Elvira R, Tan E K and Zhou Z D 2025 Three-dimensional midbrain organoids: a next-generation tool for Parkinson's disease modelling and drug discovery *Stem Cell Res. Ther.* **16** 502
[51] Grasselli S, Andolfi A, Di Lisa D and Pastorino L 2025 *In vitro* electrophysiological characterization of Parkinson's disease: challenges, advances, and future directions *Front. Neurosci.* **19** 1584555
[52] Schmidt S *et al* 2023 A reversible state of hypometabolism in a human cellular model of sporadic Parkinson's disease *Nat. Commun.* **14** 7674
[53] Schindelin J *et al* 2012 Fiji: an open-source platform for biological-image analysis *Nat. Methods* **9** 676–82
[54] Qian X, Jacob F, Song M M, Nguyen H N, Song H and Ming G-L 2018 Generation of human brain region–specific organoids using a miniaturized spinning bioreactor *Nat. Protoc.* **13** 565–80
[55] Paşca A M *et al* 2015 Functional cortical neurons and astrocytes from human pluripotent stem cells in 3D culture *Nat. Methods* **12** 671–8
[56] Yoon K-J *et al* 2017 Zika-virus-encoded NS2A disrupts mammalian cortical neurogenesis by degrading adherens junction proteins *Cell Stem Cell* **21** 349–58.e6
[57] Edelstein A D, Tsuchida M A, Amodaj N, Pinkard H, Vale R D and Stuurman N 2014 Advanced methods of microscope control using μManager software *J. Biol. Methods* **1** e10